Statistical Geometry of the turbulent ISM - I. Field lines

C.C. Evirgen[1]⋆, A. Shukurov[1], F.A. Gent[2] and A. Fletcher[1].
[1]*School of Mathematics and Statistics, Newcastle University, Newcastle upon Tyne, UK, NE1 7RU*
[2]*SP²RC, School of Mathematics and Statistics, University of Sheffield, Sheffield, UK, S3 7RH*

ABSTRACT
Abstract to be left until the end. Words, words and more words to follow but first we need a paper. There will be methods, keywords and results hinted at here.

Key words: circumstellar matter – infrared: stars.

1 INTRODUCTION

The results presented in this paper are based on simulations of the multiphase interstellar medium (ISM) reported in Gent et al. (2013a) and Gent et al. (2013b), subsequently referred to as Paper I and Paper II, respectively. In particular we consider a model, identified as B1Ωs in Paper II. Supernova(SN)-driven turbulence is applied to ISM in a section of a spiral galaxy differentially rotating, stratified about the galactic disk and subject to, radiative cooling, photoelectric heating and other transport processes. The rate and distribution of SN explosions, gravity and angular momentum are consistent with observational parameters for the solar neighbourhood. A nano Gauss seed magnetic field is applied and amplified by dynamo until it saturates with a mean magnetic stength of a few micro Gauss, remarkably consistent with observed estimates for the Milky Way.

Models of the magnetized ISM (Heitsch et al. 2001; Mac Low et al. 2005) have explored the effects of magnetic field on the localized ISM, including the fluctuation dynamo, but without the effects of stratification and the large scale structure induced by the differential rotation of the disk. Large scale structure in the stratified ISM has been investigated by de Avillez & Breitschwerdt (2005), but without differential rotation the dynamo to grow the field to full strength is absent, so an imposed field is applied. Hanasz et al. (2005); Dobbs & Price (2008) and Hanasz et al. (2009) apply magnetic fields to global disk models, including a dynamo, but due to numerical constraints must limit or exclude vertical stratification and multi-phase gas composition. Korpi et al. (1999) and Gressel et al. (2008) conducted earlier simulations with the same approach as described here, but with lower resolution and higher diffusion were unable to follow the dynamo through to saturation. The advantage of the results from Paper II is that the magnetic field produced is not imposed, but evolves dynamically under realis-

tic physical processes governing the formation of the thermo-hydrodynamic structure of the ISM. From this point of view it is of great value for appreciating the multi-phase structure of the magnetized ISM and for comparison with observation.

A snapshot of the ISM at approximately $t = 1.4$ Gyr is used. Its characteristics, in terms of the fractional volumes of the phases, is representative of the steady-state phase of the dynamo. In addition, there are two potential SN remnants, which provide isolated structures of hot gas. This enhances the illustration of the effect that hot gas has on the mean magnetic field.

The multi-phase structure is defined in terms of temperature and density. However, an equivalent definition is given in terms of entropy, which has an explicit defintion linking density and temperature (Gent 2012). The cold, warm and hot phases are defined by the entropy ranges, $s \leqslant 3.7 \cdot 10^8$, $3.7 \cdot 10^8 < s < 23.2 \cdot 10^8$ and $s > 23.2 \cdot 10^8$ erg g^{-1} K^{-1}, respectively.

2 THE MEAN MAGNETIC FIELD

When considering the mean-field decomposition of the magnetic field, the notation used by (Gent et al. 2013b) is adopted. Volume averaging with a Gaussian kernel, $G_l(\boldsymbol{x} - \boldsymbol{x}')$ is used to decompose the magnetic field, $\boldsymbol{B}$, into mean (large-scale), $\boldsymbol{B}_l$ and random (small-scale), $\boldsymbol{b}_l$, fields. The decomposition is given by

$$\boldsymbol{B} = \boldsymbol{B}_l + \boldsymbol{b}_l, \qquad \boldsymbol{B}_l = \langle \boldsymbol{B} \rangle_l. \tag{1}$$

Gaussian smoothing of the magnetic field with kernel size l is represented by

$$\langle \boldsymbol{B} \rangle_l = \int_V \boldsymbol{B}(\boldsymbol{x}')G_l(\boldsymbol{x} - \boldsymbol{x}')d^3\boldsymbol{x}', \tag{2}$$

$$G_l(\boldsymbol{x}) = (2\pi l^2)^{-3/2} \exp[-\boldsymbol{x}/(2l^2)],$$

where $l \approx 50$pc is half the integral scale of random motions (Gent et al. 2013b). This value is adopted for this paper based on the justification given in (**?**). Preliminary analysis does not show significant sensitivity of the mean or random

⋆ E-mail: c.c.evirgen@newcastle.ac.uk (CCE); anvar.shukurov@newcastle.ac.uk (AS); f.gent@shef.ac.uk (FAG); andrew.fletcher@newcastle.ac.uk (AF)

field to variations in l within the range $0 < l < 100\mathrm{pc}$. However, future work will consider analysis of isolated structures in the ISM. A more detailed analysis of length and correlation scales will be carried out. However, the current definition, $l = 50\mathrm{pc}$, is sufficient for the purposes of this paper.
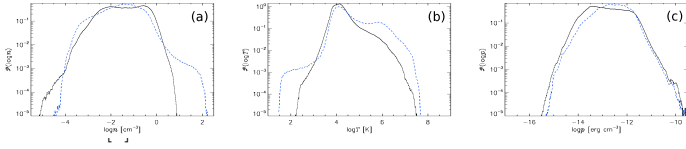
Figure 1. Volume weighted probability distributions of gas number density **(a)**, temperature **(b)** and thermal pressure **(c)** for models H1Ω (black, solid) and B1Ω (blue, dashed) for the total numerical domain $|z| \leqslant 1.12$ kpc.
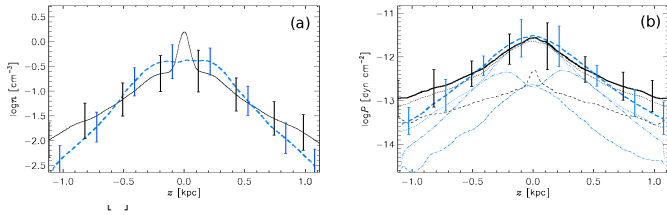

Figure 2. Horizontal averages of gas number density, $\overline{n}(z)$ **(a)**, and total pressure, $\overline{P}(z)$ **(b)**, for Model B1Ω (solid, black), and Model H1Ω (dashed, blue). Each are time-averaged using eleven snapshots respectively, spanning 100 Myr. The vertical lines indicate standard deviation within each horizontal slice. The thermal $\overline{p}(z)$ (dotted) and ram $\overline{p}_{\mathrm{turb}}(z)$ (fine dashed) pressures are also plotted **(b)**. For Model WSWah the magnetic pressure $\overline{p}_B$ is also plotted (fine, dash-3dotted).

Figure 3. Probability distributions by phase: cold (blue, dashed), warm (black, solid) and hot (red, dash-dotted) for gas number density (n **(a), (b)**) and temperature (T **(c), (d)**) for Model B1Ω **((a), (c))** and Model H1Ω **((b), (d))**. 95% confidence intervals for temporal deviation are shown as error bars.

3 THREE-PHASE STRUCTURE OF THE FIELD

The total volume probability distributions for gas number density n, temperature T and thermal pressure p are displayed in Fig. 1 from Models B1Ω (black, solid) and H1Ω (blue, dashed). Note that Model H1Ω includes the correction to the SN distribution, which stabilises the disc against unphysical cyclic oscillations, although it is still subject to natural random vertical fluctuations. Hence the mean density in the SN active region remains consistently higher than in Model WSWa.

Although the three phase temperature distribution is still visible for this model in Fig. 1b, it is less pronounced than the results from Model WSWa shown in Fig. **??**b. However the three phase structure for the MHD Model B1Ω is not at all apparent in panel b, with a significantly narrower range of temperatures. The bulk of the density distributions (a) are quite similar between the HD and MHD models, except that the high densities are not as well resolved in the MHD models. The thermal pressure distributions are very similar, but with the HD modal pressure approximately one third the MHD modal pressure.

As discussed in Section **??** the stability of the disc reduces the effectiveness of the SNe to generate and circulate hot gas, in the absence of SN clustering. Hence Model H1Ω has a slightly thicker disc, with less hot gas than Model WSWa. On top of this the effect of the magnetic pressure in Model B1Ω is to expand the thick disc even further and this is illustrated in Fig. 2a, where the horizontal averages of gas number density $n(z)$ are plotted against z for both models. The strong peak in the density at the mid-plane is evident for Model H1Ω (black, solid), while for Model B1Ω (blue, dashed) there is a broad plateau in the
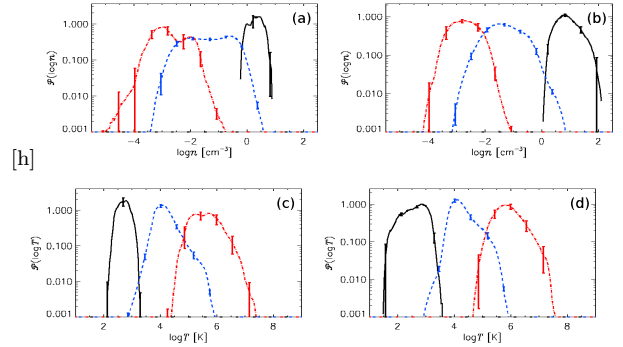
density, extending to $|z| \simeq 300$ pc, where the mean magnetic field is strongest.

The horizontal averages of the pressure are plotted in Fig. 2b for both models. There is a strong peak at the mid-plane in the turbulent pressure for the HD model (black, dashed), but a much weaker profile for the MHD model (blue, dash-dotted). There are two peaks in the magnetic pressure (blue, dash-3dotted) near $|z| \simeq 200$ pc, which supports the extended density profile. Another possible effect, which might constrain the circulation of the hot gas, and hence enhance the pressure at the mid-plane, is the strong horizontal orientation of the field. As mentioned in Section **??** the periodic boundary conditions exclude a non-zero vertical component to the mean field, so the magnetic tension predominantly acts against the vertical flows. Some understanding of the multi-phase structure of the magnetised ISM is still possible from these models, but the extreme temperatures and densities are significantly under represented. To improve this in future work it will be desirable to allow unrestricted evolution of vertical field and to apply realistic clustering of the SNe to generate more supperbubbles (composite multiple SN remnants forming a single super-structure) or chimneys (plumes venting hot gas from the disc towards the halo).

Results for separation of the ISM into three phases using the method detailed in Section **??** are shown for Models B1Ω and H1Ω in Fig 3 with total volume probability distributions. The phases are defined using entropy s such that for cold $s < 4.4 \cdot 10^8 \, \mathrm{erg \, g^{-1} \, K^{-1}}$ and hot $s > 23.2 \cdot 10^8 \, \mathrm{erg \, g^{-1} \, K^{-1}}$ with warm in between. Apart from the higher densities for the cold phase with the HD model (panel b), anticipated by the volume distributions (Fig. 1), the warm and hot distributions for the MHD density (panel a) are broad, with a bimodal structure to the hot gas. The distributions for the warm gas (panels c and d) are very similar and for the cold (hot) distributions the MHD model does not extend to as low (high) temperatures.

Comparing the combined probability distribution of density and temperature for both of these models in Fig. 4 with those of Model WSWa in Fig. **??** the spread is more broad and not obviously aligned along a line of constant pressure. The HD distribution here is less compact than
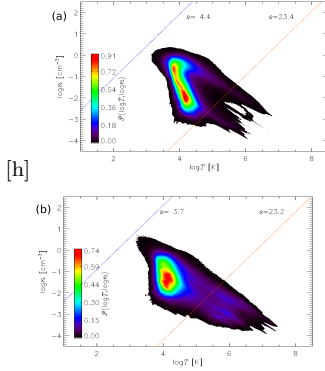
Figure 4. Probability contour plot by volume of $\log n$ vs $\log T$ for Model B1Ω **(a)** and Model H1Ω **(b)**. The lines of constant entropy $s = 4.4 \cdot 10^8$ and $23.2 \cdot 10^8$ erg g^{-1} K^{-1} indicate where the phases are defined as cold for $s \leqslant 4.4$ and as hot for $s > 23.2$.
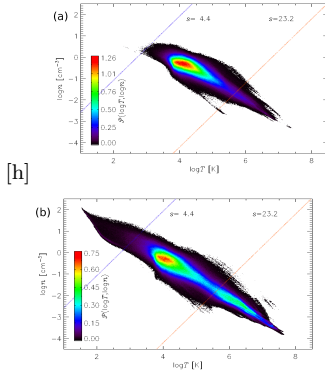

Figure 5. The mid-plane probability distributions ($|z| < 100$ pc) by gas number density $\log n$ and temperature $\log T$ for **(a)** Model B1Ω and **(b)** Model H1Ω.

with MHD. However when considering only the mid-plane distributions, as displayed in Fig. 5 the distributions match better with Model WSWa and the pressure alignment is evident. So the broad distributions for the total volumes are explained by the stronger gradient in the pressure distribution, due to the reduced stirring of the hot gas. The thermal pressure at the mid-plane is also very similar in both models, reflected also in the agreement of the total and thermal pressure near the mid-plane in the plot of horizontal averages (Fig 2b). The magnetic and turbulent pressure in Model B1Ω combine to match the mid-plane turbulent pressure alone of Model H1Ω. For the temperature in Model B1Ω the hot gas has two modes, evident in Fig. 4a at 10^5 K and 10^6 K, but at the mid-plane there only the single 10^3 K mode. The structure of the ISM at the mid-plane is therefore common to both models with modes at 10^6 K, 10^{-2} cm^{-3} and 10^4 K, 1 cm^{-3}. The cold gas is insufficiently resolved in Model B1Ω for comparison.

There is no evident dependence in the probability distributions between the MHD models differing in rotation, shear or SN rate. The models in the kinematic stage extend to lower densities and higher temperatures than either the HD Model H1Ω or the MHD models in the dynamo saturated state, and also extend to lower pressures.
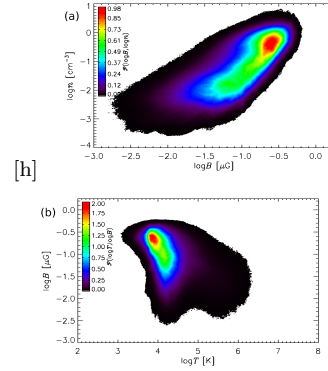

Figure 6. Total volume probability distributions ($|z| < 100$ pc) by gas number density $\log n$ and magnetic field strength $\log |B|$ **(a)** and temperature $\log |T|$ and magnetic field strength $\log |B|$ **(b)** for Model B1Ω.

In Fig. 6a the joint probability distributions of gas number density with magnetic field strength is shown and in Fig. 6b of temperature with magnetic field strength for Model B1Ω. From (a) it is clear there is a strong positive correlation between magnetic field strength and density and from (b) a weak negative correlation between temperature and field strength. The T, B distribution has very strong peak at $T = 10^4$ K.

For Model B1Ω the ISM for a single snapshot is decomposed into the three phases and the magnetic field for each plotted separately in Fig. 7. In panel a the cold gas occupies only a limited volume near the mid-plane, but the magnetic field is very strong and organised in alignment with the mean field surrounding it in the warm gas. This is represented by the length and thickness of the vector arrows. The colour of the arrows emphasises that the alignment has a strong azimuthal component. No arrows are present away from the mid-plane, because the cold gas is absent there. In panel b the warm gas is present throughout the numerical volume. Field vectors are present almost throughout and the field is highly aligned, mainly in the azimuthal direction. The strength of the field increases towards the mid-plane. The presence of some vectors in blue or grey indicates that there are significant perturbations where the field includes reversals, some of these strong. Some of the field exhibits significant vertical orientation, but it is mainly horizontal. In panel (c) the hot gas is also present throughout the volume, although in smaller amounts near the mid-plane. Despite this there is very little magnetic field. What field there is generally weak and lacks much systematic alignment, although any orientation tends to be vertical, consistent with the field lines being stretched by the gas flowing away from the mid-plane. Effectively the hot gas has a very weak field, which is highly disordered. Most of the magnetic field, and particularly the mean field, occupies the warm gas. Detailed quantitative analysis of the structure of the gas will be deferred to future work.

4   SUMMARY

The magnitude of the magnetic field is strongly aligned to the density of the ISM and indirectly the warm and cold
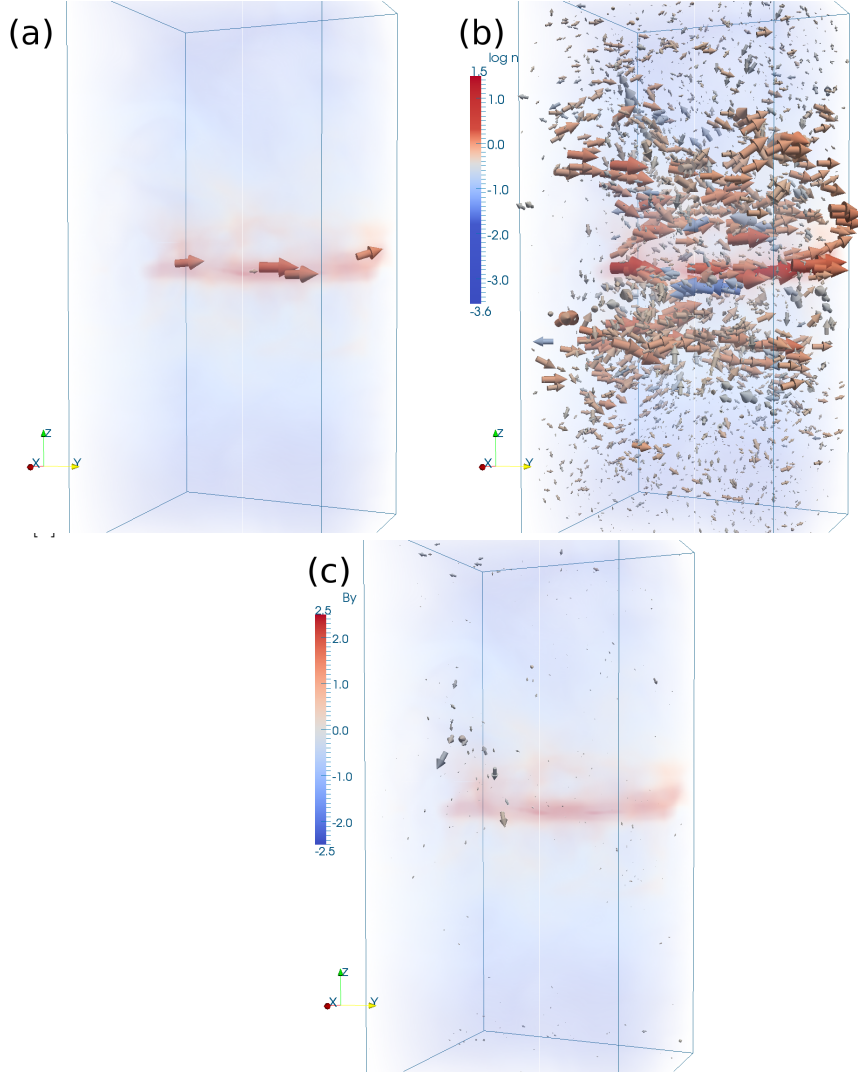
Figure 7. Vector plots of the magnetic field $\boldsymbol{B}$ (a) in the cold phase (b) the warm phase and (c) the hot phase. Field directions are indicated by arrows and strength by their thickness. The colour of the arrows indicates the strength of the azimuthal (y) component (colour bar on the right). The background shading illustrates the density of the ISM.

phases. More particularly the mean field is stronger in the warm and cold gas, with the hot gas containing a more random field. The mean magnetic field and the magnetic energy is strongest at $|z| \simeq 300\,\mathrm{pc}$, just outside the SNe active region. The fluctuating dynamo is likely to be strongest in this SNe active region, but due to the low magnetic Reynolds numbers in the simulations, it is likely that the field and energy is significantly weaker in the simulations than might be expected.

5   FIELD LINES OF THE MAGNETIC FIELD

Field lines of the magnetic field give a qualitative description of the magnetic field in the ISM. We introduce sampling of physical variables along the field lines of the magnetic field, to obtain a quantitative description of the observables. Observables, such as entropy or pulsar RM measures (**?**) are frequently used to derive other observables or statistics. The use of sampling along field lines will enable the analysis of observables across many snapshots, whilst avoiding the use of time averages, which is not sensible for observables associated to a turbulent flow (Tennekes & Lumley 1972). For example, the wavelet transform methods used by Stepanov *et al* (**?**) are used to derive the Galactic magnetic field from pulsar RM data. Field lines of the Galactic magnetic field can be derived from this analysis and it can be further analysed using sampling along the field lines.

The mean magnetic field is considered first, to explore the large-scale characteristics of the magnetic field, having extracted the random, small-scale fluctuations with Gaussian volume averaging. Intuition suggests that the mean magnetic field will prefer to stay in the warm phase, which provides a less hostile environment for the magnetic field than the transonic, compressible turbulence of the hot phase. This will be discussed using the field lines and by comparison with a test case.

5.1   Field line equation for a vector field, $A(x)$

Given a vector field, $A(x)$, in Cartesian coordinates, its field lines are described by

$$\frac{dx}{A_x} = \frac{dy}{A_y} = \frac{dz}{A_z} = ds, \tag{3}$$

where ds is a separation constant used to integrate along the field line. This is formulated as

$$\begin{cases} \frac{dx}{ds} = A_x, \\ \frac{dy}{ds} = A_y, \\ \frac{dz}{ds} = A_z, \end{cases} \tag{4}$$

The field line equation is integrated along x, y and z to obtain the field lines,

$$L : (x(s), y(s), z(s)),$$

which are integrated using a 4th-order Runge-Kutta scheme. For discrete-valued $A(x)$ interpolation is used to evaluate its components at positions, x, which do not lie on the data grid.

5.2   3D rendering of field lines of the mean magnetic field

In Figure 8 on the facing page, the white field lines have been seeded along the xz-axis at $y \approx -0.51$ kpc. The translucent gas inside the box is a representation of the log density, $\log(n)$, field. Density decreases from brighter to darker colours. Since the warm and hot phase represents approximately %99 of the fractional volume of the ISM gas, it is only useful for visualising the characteristics of the field line within the warm and hot phases. We will present a preliminary result regarding the field lines within the cold phase in this paper. However, a more detailed discussion will
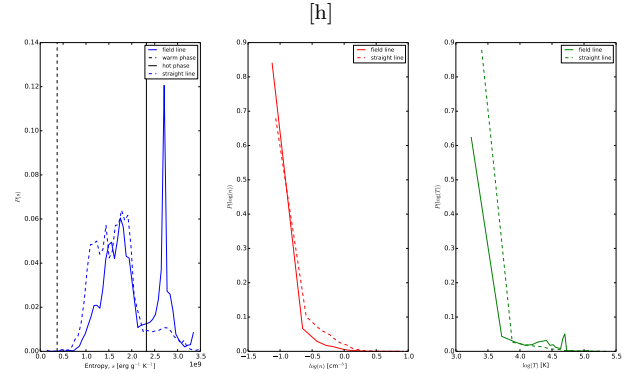

[h]

Figure 9. PDFs of entropy (blue), s, log density (red), $\log(n)$, and log temperature (green), $\log(T)$, along field lines (solid) and straight lines (dashed).

be reported elsewhere. For descriptive purposes, the yellow shades of gas correspond to warm gas and the red shades correspond to the hot phase. We note that the field lines are generally aligned with the positive y-direction, especially in the warm phase and the field lines are smooth inside the warm gas. However, we notice significant differences in the characteristics of the field lines in the hot phase.

There is an isolated structure of hot gas (likely to be a SN remnant) in the (approximate) range $-0.8 < z < -1.1$ kpc. The field lines in this region still traverse the computational domain in the positive y-direction. However, they are distorted and stretched in the positive z-direction in the region surrounding the hot gas.

Similarly, in the range $0.7 < z < 1.1$ kpc, there is a larger structure of hot gas, which spans the xy-plane. This structure appears to be part of rising hot gas, which is leaving the computational domain. As it leaves, it elongates the magnetic field lines until they are no longer connected inside the domain. Consequently, the the field lines are approximately perpendicular to the y-axis, where the stretching of the field lines occur due to the hot phase. (NEED TO CHECK WHETHER THE MAGNETIC FIELD ENERGY IS STRONGER IN THESE REGIONS COMPARED WITH THE STRAIGHT LINES!)

5.3   A Test: Comparison of probability density functions (PDFs) along field lines with PDFs along straight lines

Even though the visualisation is informative, it is necessary to determine whether the field lines are sensitive to the phases of the ISM. Consequently, we compare the characteristics of the field lines against straight lines launched in the positive y-direction, from the seed points used to compute the field lines. This test is devised using ideas from the field of stereology (Baddeley & Jensen 2004), lineal analysis in particular. The straight lines used in the test case will have the same general characteristics as the field lines, since they both traverse the computational domain in the positive y-direction. This ensures that the lines are representative of the field lines being sampled. Despite having the same general characteristics, the straight lines should not be sensitive to the phases of the ISM; they will not prefer to stay in a particular phase, whilst
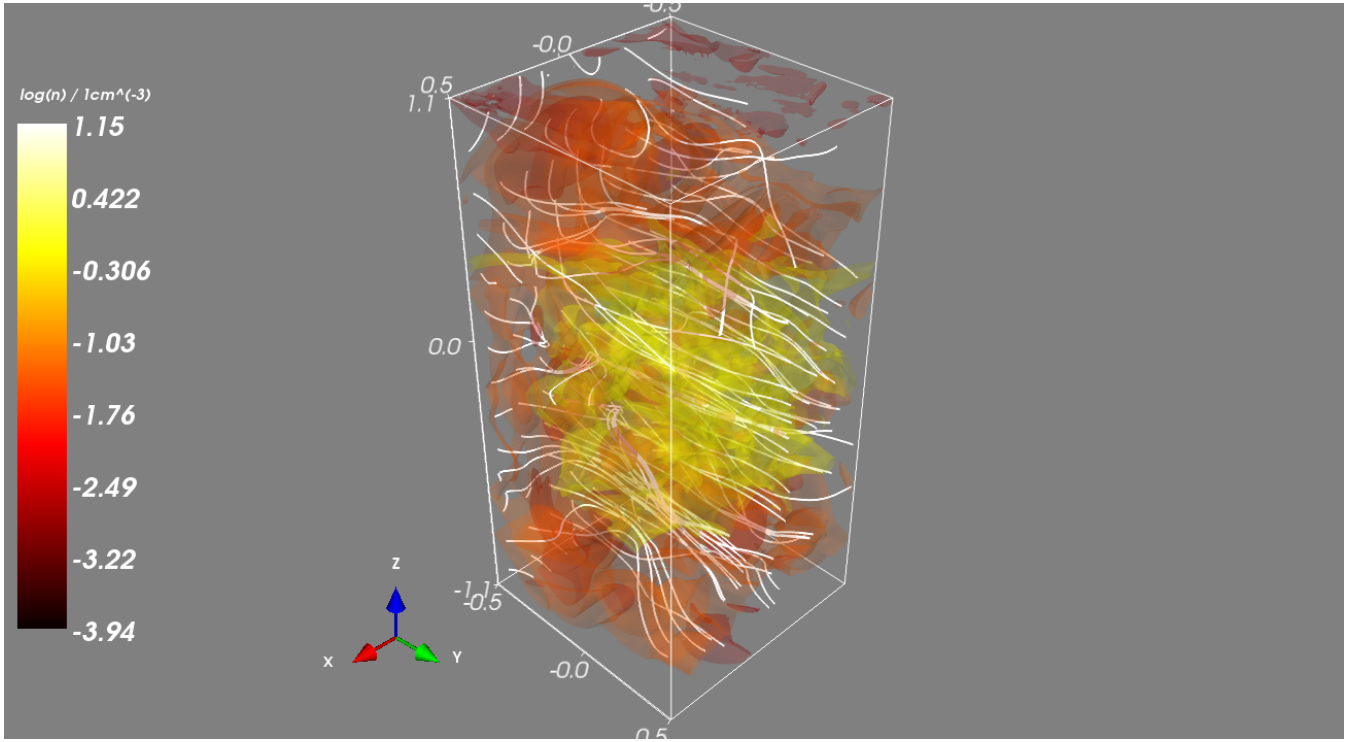
Figure 8. 3D rendering of the field lines of the mean magnetic field. The white lines are field lines seeded along a regular grid on the *xz*-plane at $y \approx -0.5$ kpc.

avoiding others. Therefore, comparison of the PDFs of the observables sampled along the field lines and the straight lines, should identify sensitivity (or lack thereof) of the field lines to the phases of the ISM.

Figure 9 on the preceding page shows the probability density functions (PDFs) of entropy, log density and log temperature sampled along field lines (solid lines) and straight lines (dashed lines). The PDFs for log density and log temperature suggest that the PDFs have similar overall behaviour, which is most likely due to their alignment in the *y*-direction. This is reassuring since the choice of aligning the straight lines in the *y*-direction was to avoid introducing uncharacteristic behaviour into the comparison. The straight lines have the orientation of the field lines, without the sensitivity to phases.

We now consider the PDFs entropy along the field lines and straight lines in Figure 9. These PDFs are more rich in information. Firstly, we observe similar peaks in the region $1.66 < s < 10.365$, which corresponds to the warm phase. This agrees with Figure 8 in that the field lines do not seem sensitive to the warm phase.

Probability	Field lines	Straight lines
$\mathcal{P}$(cold phase)	$8.384 \cdot 10^{-5}$	$7.818 \cdot 10^{-4}$
$\mathcal{P}$(warm phase)	0.6577	0.8865
$\mathcal{P}$(hot phase)	0.3422	0.1127

Table 1: Respective probabilities of finding the field and straight in the cold, warm and hot phases.

We observe a sharp peak for the PDF of entropy along the field line, centred at $s \approx 27 \cdot 10^8$ erg g^{-1} K^{-1}, which is inside the hot phase. A similar peak is not observed for the PDF of entropy along the straight line. This can be explained by the field lines being stretched by the hot gas and thus traversing the hot phase for a higher proportion of their length than the straight lines, which are not affected by stretching. We formulate probabilities of traversing each phase for the field lines and straight lines from their PDFs. The probabilities are expressed as,

$$\mathcal{P}(\text{cold phase}) \equiv \mathcal{P}(s \leqslant 3.7 \cdot 10^8),$$
$$\mathcal{P}(\text{warm phase}) \equiv \mathcal{P}(3.7 \cdot 10^8 < s < 23.2 \cdot 10^8), \quad (5)$$
$$\mathcal{P}(\text{hot phase}) \equiv \mathcal{P}(s > 23.2 \cdot 10^8).$$

The probabilities of traversing the phases, for the field lines and straight lines, are given in 1. We observe that the probabilities of the straight lines traversing each phase closely match the fractional volumes of the phases, as expected; lines that are not sensitive should traverse each phase with probability proportional to the fractional volume. On the other hand, the probability of a field line traversing the hot phase is significantly higher than that of a straight line, which reiterates the effect of the stretching of field lines by the phase. The probability of a field line traversing the warm phase is lower than that of a straight line. However, this is a direct consequence of the distortion of the magnetic field by the hot phase. We note that the probability of a field line traversing the cold phase is lower than that of a straight line by an order of magnitude. This could constitute a preliminary indication that the field lines avoid the cold phase. As
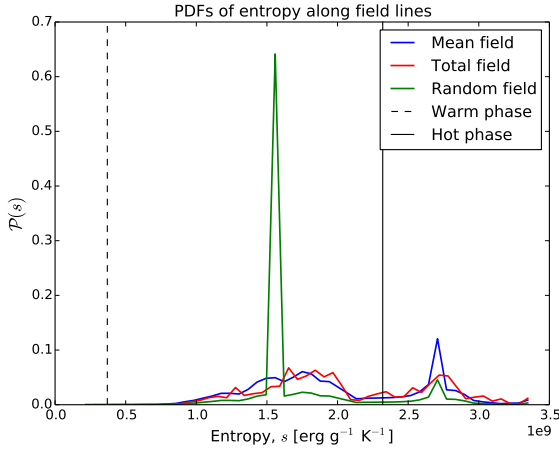
Figure 10. PDFs of s along field lines of the mean (blue solid), total (red solid) and random (green solid) fields. The boundaries of between the cold and warm phases (black dashed) and between the warm and hot phases (black solid) are indicated.

noted earlier, the characteristics of the magnetic field in the cold phase will be explored in greater detail elsewhere.

5.4 Field lines of the total and random magnetic field

We use Equation (3) to construct field lines for the total and random magnetic field using the same method as for field lines of the mean magnetic field. Sampling along these lines is used to obtain the PDF of entropy, as seen in the previous section for the mean magnetic field. PDFs of log density and log temperature have been omitted, since the PDF of entropy contains sufficient detail to understand the characteristics of the field lines. The comparison with PDFs along straight lines are only relevant for field lines of the mean magnetic field. This section focuses on the comparison of PDFs along the total, mean and random magnetic field. Figure 10 shows these PDFs. FIrstly, we note that all of the PDFs are clustered in the warm and hot phases. However, this is inextricably linked to the fractional volumes of the phases. It is difficult to discuss whether avoidance of the cold phase by the field line is also a contributing factor.

We concentrate on the warm and hot phases. The PDF for the total field is similar to that of the mean field in the warm phase. They both have a smooth distribution, even though the PDF of the total appears to be slightly more skewed. In the hot phase, the PDF for the total field is smooth. However, The PDF of the mean field peaks sharply, at approximately $s = 27 \cdot 10^8$ erg g^{-1} K^{-1}. Even though the PDF for the total field is smooth, its local maxima is close to this value of s. A similarly sharp peak is observed in this region for the PDF of the random field. This could suggest that $s = 27 \cdot 10^8$ erg g^{-1} K^{-1} is a characteristic entropy associated with the hot phase for this snapshot.

A sharp peak is also observed in the warm phase in the PDF for the random field, at approximately $s = 15.5 \cdot 10^8$ erg g^{-1} K^{-1}. The probability density for the random field is weak outside of the sharp regions. It appears that the random field is characterised by a small range of entropy values in the warm and hot phases.

5.5 Curve fitting for PDFs of entropy

6 CONCLUSIONS

REFERENCES

Baddeley A., Jensen E., 2004, Stereology for Statisticians. Chapman & Hall/CRC Monographs on Statistics & Applied Probability, Taylor & Francis

de Avillez M. A., Breitschwerdt D., 2005, A&A, 436, 585

Dobbs C. L., Price D. J., 2008, MNRAS, 383, 497

Gent F. A., 2012, PhD thesis, Newcastle University School of Mathematics and Statistics

Gent F. A., Shukurov A., Sarson A., Fletcher G. R., Mantere M. J., 2013a, MNRAS, 432, 1396

Gent F. A., Shukurov A., Sarson G. R., Fletcher A., Mantere M. J., 2013b, MNRAS, 430, L40

Gressel O., Elstner D., Ziegler U., Rüdiger G., 2008, A&A, 486, L35

Hanasz M., Lesch H., Otimianowska-Mazur K., Kowal G., 2005, in Chyży K., Otmianowska-Mazur K., Soida M., Dettmar R.-J., eds, The Magnetized Plasma in Galaxy Evolution Cosmic-ray-driven dynamo in galactic discs. Jagiellonian University, Kraków, pp 162–170

Hanasz M., Wóltański D., Kowalik K., 2009, ApJ, 706, L155

Heitsch F., Mac Low M.-M., Klessen R. S., 2001, ApJ, 547, 280

Korpi M. J., Brandenburg A., Shukurov A., Tuominen I., 1999, A&A, 350, 230

Mac Low M.-M., Balsara D. S., Kim J., de Avillez M. A., 2005, ApJ, 626, 864

Tennekes H., Lumley J. L., 1972, First Course in Turbulence. Cambridge: MIT Press